ADVANCES IN ATMOSPHERIC SCIENCES, VOL. 25, NO. 2, 2008, 253–266

Deduction of the Sensible Heat Flux from SODAR Data

PAN Naixian* (潘乃先) and LI Chengcai (李成才)

Department of Atmospheric Sciences, School of Physics, Peking University, Beijing 100871

(Received 26 September 2006; revised 15 May 2007)

ABSTRACT

A new method for deduction of the sensible heat flux is validated with three sets of published SODAR (sound detection and ranging) data. Although the related expressions have previously been confirmed by the author with surface layer data, they have not yet been validated with observations from the boundary layer before this work. In the study, selected SODAR data are used to test the method for the convective boundary layer. The sensible heat flux (SHF) retrieved from SODAR data is found to decrease linearly with height in the mixed layer. The surface sensible heat fluxes derived from the deduced sensible heat flux profiles under convective conditions agree well with those measured by the eddy correlation method. The characteristics of SHF profiles deduced from SODAR data in different places reflect the background meteorology and terrain. The upper part of the SHF profile (SHFP) for a complicated terrain is found to have a different slope from the lower part. It is suggested that the former reflects the advective characteristic of turbulence in upwind topography. A similarity relationship for the estimation of SHFP in a well mixed layer with surface SHF and zero-heat-flux layer height is presented.

Key words: mixed layer, sensible heat flux, similarity relationship, SODAR, zero-heat-flux layer

DOI: 10.1007/s00376-008-0253-8

1. Introduction

The boundary layer is one of the most important parts of the Earth-atmosphere system in which we live, with direct effects on our daily life and work. It also plays a central role in the exchange of heat, moisture, momentum, trace gasses and aerosols between land, ocean, and ice surfaces, in cloud formation, and in the general circulation of the atmosphere. The parameterization of turbulence for numerical modeling has been a strong motivation for the development of in situ experimental studies of boundary layer meteorology. One of the major problems in atmospheric physics is the energy budget. This problem cannot be solved without measuring fluxes at the Earth's surface, where radiative energy is converted into sensible heat and latent heat. Weather modeling requires these boundary conditions (energy and momentum fluxes) at a spatial scale compatible with the size of the mesh, i.e., over surfaces whose scale ranges from 10–100 km. To provide this scale integration and to take into account landscape diversity is a challenge for atmospheric research. Then the observations and researches on such heat fluxes, e.g., sensible heat flux (SHF), which is a very crucial parameter in the study of boundary layer meteorology, in various scales, including measurements at ground-based stations or aboard aircrafts, have been carried out by many scientists (Panofsky et al., 1977; Coulter and Wesley, 1980; Hill et al., 1992; Thiermann and Grassl, 1992; Bian et al., 2003; Li et al., 2006). Although *in situ* measurements provide comparatively accurate results, they are costly to carry out over long periods and the data may not be representative spatially and temporally (Wyngaard, 1990). Remote sensing technology of SHF and other turbulent parameters has been an area of interest since the 1980s. Remote sensing techniques usually offer continuity in observations over both space and time, and one such technique is scintillometry. The structure parameter of refractive index C_n^2, at a given wavelength, can be deduced by measuring the fluctuations of a beam of light along a path. In the visible to mid-infrared region, the variation of C_n^2 mainly depends on temperature fluctuations, i.e., C_T^2. From C_T^2 measured in the atmospheric surface layer, SHFs can be deduced using simplified equations for turbulent kinetic energy and temperature variance budgets (inertial dissipation method) (Thiermann and Grassl,

*Corresponding author: PAN Naixian, nxpan@pku.edu.cn

1992; Hill et al., 1992). The scintillometry technique provides a path-averaged measurement of SHFs in the surface layer and was tested over a heterogeneous area for determination of area-averaged SHFs (Meijninger et al., 2002). Another remote sensing technique used in boundary layer meteorological detection is the acoustic sounding technique, which is a technique that offers continuity over both space and time by employing interaction of acoustic waves with the air in the lower atmosphere. This technique has been extensively used to study the microstructure of the planetary boundary layer (Singal, 1989). SODAR (sound detection and ranging) was first used three decades ago to evaluate turbulent parameters. Its usage is not limited to the surface layer, unlike the scintillation method, but instead extends to the boundary layer, including the temperature structure coefficient C_T^2, energy dissipation rate ε, velocity structure coefficient C_V^2, and vertical velocity variance σ_w^2 based on the SODAR equation or the Doppler shift in frequency of echo signal (Neff, 1975; Gaynor, 1977; Weill et al., 1978). On the basis of similarity theory (Panofsky et al., 1977) and under the assumption that local mechanical production is negligible, Weill et al. (1980) presented a method of vertical velocity variance for evaluation of surface SHF in a dry and well mixed layer. Surface SHF can then be evaluated by extrapolating the linear part of the σ_w^3/z profile to the surface layer ($z = 0$). Meanwhile, Coulter and Wesley (1980) presented a method of temperature structure coefficient based on a similarity relationship of C_T^2 [see Eq. (12) below]. However, the applicability from the above two studies is limited to a short period on a clear day and over a flat area. Further studies have been made along these lines. It has been found that local mechanical production cannot usually be neglected and the C_T^2 profiles measured by SODAR do not always meet the $z^{-4/3}$ law in the mixed layer. In the early part of the day, some remarkable differences occurred between estimated heat flux and direct measured values because of the absence of free convection (Keder et al., 1989; Vogt and Thomas, 1994).

Pan (2002) presented two equations of SHF based on a dimensional analysis. Either one can be used to determine the sensible heat flux profile (SHFP) with the quantities measured or estimated by SODAR. The equations were confirmed with data from the surface layer (Pan, 2002). In this paper, parts of the published data measured in the convective boundary layer are used to verify this method. In section 2 some related quantitative measurements of turbulent parameters by SODAR are presented. In particular, the main factors that introduce errors in the measurements of radial wind velocity and echo intensity in SODAR detection are reviewed. Then, in section 3, the methodology used for the retrieval of SHFs is presented. Data processing from three studies is described in section 4. Section 5 presents the results of derived SHFs from the above data and methodology, as along with some associated discussion. The deduced surface SHFs are compared to those from direct measurements, and the deduced SHFPs for different terrain are analyzed. The representative surface SHF and related similarity relationship is discussed in section 6. Finally, in section 7, conclusions of the study are drawn.

2. Quantitative measurements of turbulent parameters by SODAR

2.1 *Measurement of the temperature structure coefficient*

The effective scattering cross section of scattered acoustic waves is related to the fluctuations of temperature and humidity (rewritten from Ostashev, 1994):

$$\sigma(\theta) = 0.030k^{1/3}\left(\sin\frac{\theta}{2}\right)^{-11/3}\left\{0.136\left[\cos^2\theta\frac{C_T^2}{T^2} + 2(0.596\cos\theta - 0.095)\cos\theta\frac{C_{qT}}{T} + (0.596\cos\theta - 0.095)^2 C_q^2\right] + \cos^2\frac{\theta}{2}\cos^2\theta\frac{C_V^2}{c^2}\right\}, \quad (1)$$

where θ is scattering angle, k is wave number, c is sound speed, T is air temperature, C_q^2 is the humidity structure coefficient, and C_{qT} is the co-structure coefficient of humidity and temperature. In dry air, the products of humidity can be neglected and from Eq. (1) it is immediately apparent that C_T^2 can be determined by measurement of the backscattered energy ($\theta = \pi$):

$$\sigma(\pi) = 0.00408k^{1/3}\frac{C_T^2}{T^2}. \quad (2)$$

The SODAR equation of monostatic mode can be expressed by the following equations (Pan, 1997):

$$P_\mathrm{r} = P_\mathrm{t}\frac{c\tau AG}{2R^2}\sigma(\pi)\alpha_\mathrm{w}T_\mathrm{a}T_\mathrm{e} \quad (3a)$$

$$= c_\mathrm{s}\frac{1}{R^2}C_T^2\alpha_\mathrm{w}T_\mathrm{a}T_\mathrm{e}, \quad (3b)$$

where P_r is the received sound power, P_t is the transmitting sound power, τ is the transmitting pulse length, G is the antenna gain, A is the antenna aper-

ture, R is the range from antenna to scattering volume, c_s is a constant composed of parameters for the SODAR system, α_w is the wind attenuation factor, T_a is the transmissivity of sound intensity for the atmospheric absorption, and T_e is the transmissivity for the excess attenuation. The wind attenuation factor is defined as the ratio of received echo power with wind to that with no wind (Pan, 1997):

$$\alpha_w = \frac{2}{\pi}\left[\arccos\left(\frac{\psi}{\gamma}\right) - \frac{\psi}{\gamma}\sqrt{1-\left(\frac{\psi}{\gamma}\right)^2}\right], \quad (4)$$

where ψ is the arrival angle of the echo signal and γ is the beam angle.

The temperature structure coefficient, C_T^2, can then be estimated by measuring the echo intensity and correcting it for the attenuation. The accuracy of estimates depends on the calibration of SODAR parameters in the right side of Eq. (3a) and the correction of wind effect, atmospheric absorption and excess attenuation for the received signal.

One method for calibration involves measuring the response of the system to a known signal (determined with a calibrated microphone) and measuring the output power of the transmitter (Sisterson and Coulter, 1979). This method requires care and attention to the beam pattern and the exact geometry of the transmitter, receiver and microphone. A second is to make simultaneous measurements of returned signal strength and direct measurements of C_T^2, which was successful in the Gaomeigu experiment (Pan, 2002). The calibration was made just before the experiment started, which may avoid the possible inherent variability of the acoustic transducer during a long storage, under neutral condition with a light wind.

The wind effect may be overestimated by Eq. (4) because of the assumption of a conoid acoustic beam with uniform energy distribution on beam sections. This correction, however, is useful for strong wind. Atmospheric attenuation of acoustic waves has often been ignored in data processing. In fact, atmospheric absorption and excess attenuation are both important in the evaluation of C_T^2 with a reasonable accuracy. The authors' studies show that the excess attenuation has been largely underestimated. The new expression of excess attenuation coefficient (Pan, 2003) is:

$$a_e = \frac{L_e^{5/3}}{\lambda^2}\left(2.9\frac{C_V^2}{c^2} + 0.40\frac{C_T^2}{T^2}\right), \quad (5)$$

where L_e is the effective turbulent outer scale, and written as:

$$L_e = R\tan\left(\frac{\gamma}{2}\right), \quad (6)$$

where R is the distance from the source to the scattering volume and γ is the angular beam width. The excess attenuation coefficient is then sensitive to L_e and increases with the distance for a conical beam even in a homogeneous turbulent field. The excess attenuation of a beam-type acoustic wave is not reversible during forward propagating in the turbulent atmosphere. In other words, the reversibility of the excess attenuation does not exist between the transmitter and the receiver at the two ends of a path. The transmissivity, T_e, should expressed as:

$$T_e = \exp\left(-\int_0^R a_e dr - \int_R^0 a_e' dr\right), \quad (7)$$

where a_e is the excess attenuation coefficient for the transmitting wave in m^{-1} and a_e' is the excess attenuation coefficient for the back scattered wave.

In humid air, the effect of inhomogeneity of humidity and the cooperative effect of the temperature and humidity play the same role as the effect of the inhomogeneity of temperature in the detection of SODAR (Zhou et al., 1981). The estimates of C_T^2 may have a large error in this situation.

2.2 *Measurement of the parameters in the turbulent velocity field*

2.2.1 *Vertical velocity*

There are several factors that introduce errors in the estimation of the average radial wind velocity in a measurement gate of SODAR. These errors are mainly caused by refraction of the acoustic beam (Georges and Clifford, 1974; Spizzichino, 1974); the transverse wind effect (Pan and Zheng, 1986); and the non-uniform distribution of eddies, which scatter the incident acoustic waves, within the beam sampling volume. For example, in the convective boundary layer C_T^2 is generally larger in actively rising air as it mixes with the cooler air above; when the sample volume encompasses both rising and descending air, rising portions may dominate the signal. The effect of horizontal wind on the measurements of vertical wind is complicated in the field. The vertical velocity measured by SODAR, w_x, is affected by horizontal (transverse) wind as follows (Pan and Zheng, 1986):

$$w_s = w + |\boldsymbol{U}| \cdot \frac{|\langle \boldsymbol{U}(z)\rangle|}{c}, \quad (8)$$

where w is true vertical wind, $|\boldsymbol{U}|$ is the speed of horizontal wind at height z, and $|\langle \boldsymbol{U}(z)\rangle|$ is the speed of average horizontal wind (vector) from surface to z level. It is apparent that the error of estimates of vertical wind will be too large for strong wind (say > 5 m s^{-1}) and small vertical velocity (say < 0.2 m s^{-1}), if no correction is made. However, unfortunately

Eq. (8) has not been validated by experiments and the errors caused by transverse wind are not well understood. Anyway, under low horizontal wind and for a well designed system, these factors are not as significant as the effects of environmental or system noise (Spizzichino, 1974) for the estimation of the vertical velocity. A time series record of the ratio of signal to noise is always necessary, otherwise there is an increase of fluctuation energy due to the noise effect. The bad data, which corresponds to the periods with critical low signal to noise ratio, must be eliminated.

2.2.2 *Second moments (variance and structure coefficient)*

The variance σ_{w}^2 is calculated from a series of estimates of w. The estimate of w can be determined from a single average of a number of spectra. If, however, spectra are averaged, some information about the variance will be lost because of the averaging process. On the other hand, averaging over several spectra can potentially provide a better estimate for each value. The calculation of second moments of velocity using the average velocity values in the gate volume leads to a loss of energy despite the frequency aliased energy, since this procedure is equivalent to a low-pass filtering (Finkelstein et al., 1986; Kristensen and Gaynor, 1986; Chintawongvanich et al., 1989). Kalogiros et al. (1999) presented the detail of evaluating σ_{w}^2, including the volume averaging correction. The fluctuation of transverse wind speed causes estimates of the variance of the echo spectrum to be overestimated (Pan, 1997).

The velocity structure coefficient

$$C_V^2 = \frac{\langle [V(x+r) - V(x)]^2 \rangle}{r^{2/3}} \tag{9}$$

can be determined by the difference in vertical velocity between two range gates and the distance, r, of these two gates which is within the inertial sub-range of turbulence. It can also be calculated from the difference in vertical velocity between values at the same range gate but separated in time. The value of r in Eq. (9) is now determined by the product of the horizontal wind speed and separation time between transmitting pulses. The implicit assumption in this type of calculation is that the horizontal wind speed is constant over the averaging time. Care must be taken to account for the overlap of portions of the signals from neighboring samples (Coulter, 1990). This effect can lead to significant underestimates.

3. Methodology for retrieval of SHF

Parameterization is generally used for the evaluation of fluxes in the atmospheric boundary layer, particularly in the surface layer. In remote sensing of SHF, parameterized relations are widely used. The author presented two equations of SHF based on a dimensional analysis as follows (Pan, 2002):

$$\overline{w'T'} = \alpha \sqrt{C_T^2 \sigma_{\mathrm{w}}^2}\, z^{1/3} \frac{z_0 - z}{z_i} \tag{10}$$

and

$$\overline{w'T'} = \alpha \sqrt{C_T^2 C_V^2}\, z^{2/3} \frac{z_0 - z}{z_i}\,, \tag{11}$$

where C_T^2 is the coefficient of temperature structure, σ_{w}^2 is the variance of velocity, C_V^2 is the coefficient of velocity structure, z_0 is the height of the zero-heat-flux layer, z_i is the height of the mixed layer, z is the height variable and $(z_0 - z)/z_i$ is the nondimensional height factor, and $\alpha = 1$.

Different from general parameterized expressions for the surface layer, there are no average meteorological parameters and its gradients or other scale parameters, such as friction velocity, u_*, Obukhov length L etc., in Eqs. (10) and (11). They only include the statistic turbulent parameters and a height factor, which is an empirical parameter. It implies that Eqs. (10) and (11) show a possible dynamic balance relationship between the SHF, C_T^2 and C_V^2 or σ_{w}^2 in the local homogeneous and isotropic turbulent field and that this balance does not directly relate to the average meteorological field. On the right side of the equations, the profiles of $C_T^2, \sigma_{\mathrm{w}}^2$ and C_V^2 can be obtained by a monostatic SODAR or a bistatic SODAR. The height of the mixed layer, z_i, can be determined by a visual inspection of the echo pattern. In general, the temperature inversion layers are associated with a strong backscattered acoustic signal. In particular, the maximum echo value is received from the elevated inversion layer, the base of which acts as the roof of the mixed layer. Thus, the height of the inversion layer base can be treated as the height of the mixed layer. Of course, it is easier and more accurate to find the mixed height from a SODAR-detected C_T^2 profile which has a maximum at the upper part of mixed layer. The agreement between the two methods is quite good (Asimakopoulos et al., 2004). The height of the zero-heat-flux layer, z_0, can be obtained by choosing the height where the C_T^2 profile has its minimum in the middle part of the mixed layer or is inferred empirically from the echo patterns by finding the weakest echo area in the middle part of the mixed layer (Appendix A). The error of estimates may be large when the echo pattern is complicated. The SHF can then be deduced from Eq. (10) or (11) without any help from other equipment.

4. Data processing

It is difficult to find some ideal published data for the verification of Eqs. (10) and (11). This paper encompasses some relevant data obtained in studies by Moulsley et al. (1981), Sorbjan et al. (1991) and Kalogiros et al. (1999). The data were carefully corrected by the authors to ensure quality control and quality assessment. The corrections in atmospheric absorption, excess attenuation and wind effect were finished by the present authors when any one of the three aspects had not been considered to correct the original data.

4.1 *Data from Moulsley et al. (1981)*

The experiment was carried out in June 1977. The data includes C_t^2, C_v^2, profiles, SODAR echo patterns, and direct measured parameters such as temperature, humidity, wind speed and SHF. Only the datasets of Runs 2a and 2b from Moulsley et al. (1981) were used in data processing, as the others do not include measured SHF values and corresponding echo patterns in the mixed layer. The meteorological parameters relative to Runs 2a and 2b are listed in Table 1. The SODAR parameters used in the data processing include frequency (f=2048 Hz), beam width ($B_\mathrm{w} = 9°$), and the diameter of antenna ($d \approx 1$ m). To calculate the SHF with Eq. (11), the values of C_T^2 and C_V^2 at different heights were read from corresponding profiles in Figs. 7 and 8 of Moulsley et al. (1981). The values of C_T^2 had been corrected for the atmospheric absorption by Moulsley et al. (1981) but needed further correction for excess attenuation and wind effect. Equations (2), (3) and (5)–(7) were used to correct the C_T^2 profiles for excess attenuation. With regard to the wind effect, Eqs. (3) and (4) from Pan (1997) were used to correct the C_T^2 profiles. The final corrected C_T^2 profiles are shown in Fig. 1a. The profiles are shown in Fig. 1b, which are reproduced from Moulsley et al. (1981).

Unfortunately, the published data do not include the mixed layer height, z_i, nor the height of the zero-heat-flux layer, z_0. The authors also cannot infer z_i and z_0 from the echo pattern because there is no evident capping inversion shown on the facsimile record (see Fig. 2, which presents the echo patterns of Runs 2a and 2b). To determine z_i and z_0, the direct measured values of SHF at 40 m and 137 m (Table 1) and corresponding values of C_T^2 and C_V^2, which are read from corresponding profiles, are used in Eq. (11). To avoid a possible large error on individual measured values and to improve its representation in statistics, the values of C_T^2 and C_V^2 at corresponding heights on the power fit curves (solid line in Fig. 1) are used instead of the measured values. The values of z_i and z_0 deduced from Eq. (11) and related parameters are listed in Table 2. Inserting the values of C_T^2, C_V^2, z_i, z_0 and z into Eq. (11), the SHFP is then obtained.

4.2 *Data from Kalogiros et al. (1999)*

The similarity method was used by Kalogiros et al. (1999) to analyze the σ_w^2 and C_V^2 profiles measured by SODAR. The analysis produced indirect estimates of the mixed layer parameters (the surface SHF H_0, the friction velocity and the mixed layer height z_i). The data were collected during the summer of 1993 on the top of a hill of the National Observatory of Athens in the center of the urban area of Athens, and during the summer of 1995 at a flat, rural area of Messogia Plain.

The height of the zero-heat-flux layer can be estimated with facsimile records, which is usually taken from the middle of the area in most weak echoes. The judgment from echo images may bring errors to the estimates of z_0. However, the error is estimated as being less than around 10% in this case. The possible errors of deduced SHF due to ±10% of z_0 are in the acceptable range and will be estimated carefully in the study.

Another difficulty is that there is no C_T^2 profile shown in Kalogiros et al. (1999). To produce corresponding C_T^2 profiles in convective conditions, a similarity relationship of C_T^2 may be used according to Wyngaard and LeMone (1980):

$$C_T^2 = 2.7 H_0^{4/3} \left(\frac{g}{T}\right)^{-2/3} z^{-4/3}\,, \qquad (12)$$

where H_0 is surface SHF, T is temperature and g is gravitational acceleration. This relationship was first observed in the surface layer, but also found to hold well beyond the surface layer under convective conditions (Tsvang, 1969; Neff, 1975). According to the season and time periods of the experiments carried out, the temperature T in Eq. (12) is estimated as 25°C. Even if this estimate has an error of ±5°C, the induced subjective error will be less than ±1.3% of the C_T^2 and can be neglected. The values of the surface SHF, which were directly measured using the eddy correlation method (EC), are 0.097 and 0.11 K m s^{-1} for the date 30 May 1993 and 4 September 1995 respectively. The values of z_i in Eqs. (10) and (11) are 440 m and 570 m for the experiments on 30 May 1993 and 4 September 1995 respectively, which were deduced from the heights of the local maximum of the echo intensity profiles by Kalogiros et al. (1999). The corresponding heights of the zero-heat-flux layer, z_0, are estimated with the echo pattern subjectively, which are 320 m and 350 m respectively. The SHFPs can then be obtained from Eqs. (10) and (11).

Fairall (1987) presented a model of scalar struc-

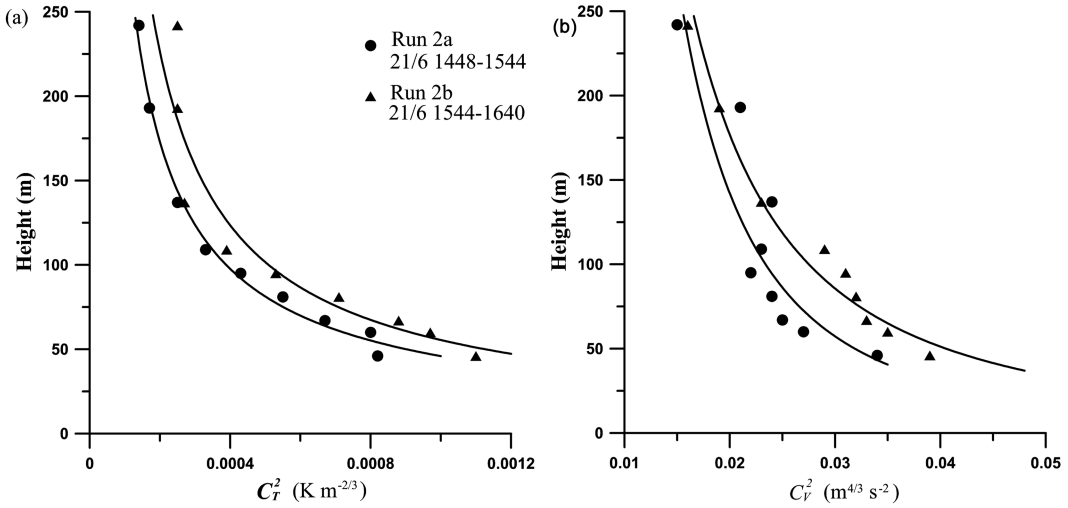

Fig. 1. (a) C_T^2 and (b) C_V^2 profiles in the mixed layer, 1977. Solid lines are the power-fitted curves.

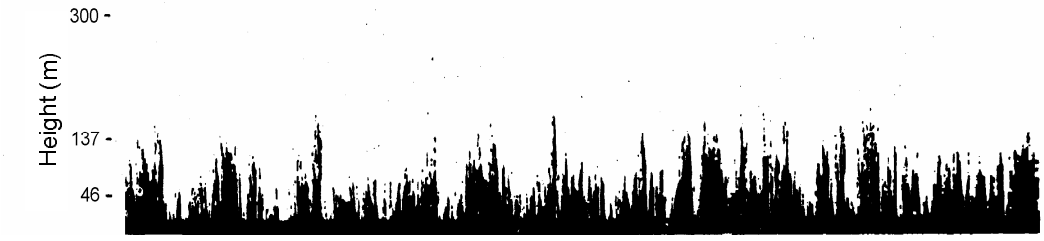

Fig. 2. Echo patterns of Run 2a and 2b, 1448–1640 UTC 21 June 1977 (Moulsley et al., 1981).

Table 1. A summary of the meteorological parameters of the experimental runs [selected from Table 2 in Moulsley et al. (1981)], 1448–1640 UTC, 21 June 1977.

Run	Amount of clouds	Height (m)	Temperature (°C)	Wind speed (m s^{-1})	Wind direction	SHF (W m^{-2})
2a	7/8	46	12.3	4.6	55°	34
		137	11.2	5.4		8
2b	7/8	46	12.9	5.0	60°	68
		137	11.8	5.7		18

Table 2. Deduced z_i, z_0 from Eq. (11) and related parameters, 1448–1640 UTC 21 June 1977.

Run	z_i (m)	z_0 (m)	Height (m)	C_T^2 (K^2 m$^{-2/3}$)	C_T^2 fitted	C_T^2 (m$^{4/3}$ s^{-2})	C_V^2 fitted	Heat flux (K m s^{-1})
2a	336	174	46	0.0008	0.0010	0.034	0.03	0.028
			137	2	0.0002	0.024	3	0.006
2b	223	181	46	0.0002	6	0.039	0.02	6
			137	5	0.0012	0.023	0	0.056
				0.0011	4		0.04	0.015
				0.0002	0.0003		2	
				7	6		0.02	
							3	

Table 3. Surface sensible heat fluxes derived from different methods.

Time	Amount of Cloud	Surface SHF (K m s^{-1})			
		SHFP	EC	C_V^2 profile	σ_W^2 profile
1448–1544[a]	7/8	0.035	–	–	–
1544–1640[a]	7/8	0.069	–	–	–
1544–1640[a]	7/8	0.069	–	–	–
1450–1535[b]	Clear	0.095	0.097	–	0.074
1017–1047[b]	Clear	0.12	0.11	0.08	0.12
1000–1015[c]	Clear	0.055	0.080	0.044[d]	0.58[e]
1145–1200[c]	Clear	0.064	0.099	0.067[d]	0.103[e]

Note: [a]Moulsley et al. (1981); [b]Kalogiros et al. (1999); [c]Sorbjan et al. (1991); [d]Local similarity theory; [e]Turbulence variance.

Table 4. Parameters (from Sorbjan et al., 1991) used in verification of Eq. (10).

Date (1987)	Time (CDT)	z_i (m)	z_0 (m)	T (°C)	Wind speed (m s^{-1})	Vapor (hPa)	RH (%)
27 June	1000–1015	315	230	22.5	6.3	16.5	55
	1145–1200	615	350	25.5	5.4	17.9	61

ture function parameters in the entraining convective boundary. The C_T^2 profiles can also be derived from Eqs. (22), (23a–c) and (36) in Fairall's (1987) paper. Besides the parameters T, H_0 and z_i above, the friction velocity u_* is necessary for the derivation of C_T^2. In the study by Kalogiros et al. (1999), the u_* can only be found in Fig. 4c for the data on 4 September 1995. Then there is u_*=0.278 m s^{-1} and an Obukhov length of $L = -14.9$ m. The results will be compared with the SHFP derived from Eq. (12) in section 5.2.

4.3 *Data from Sorbjan et al. (1991)*

The experiments were carried out during the first ISLSCP field experiment in 1987. The SODAR was located approximately 150 m east of the instrument tower used to take the surface layer measurements. Within 300 m of this location, the terrain was relatively flat, in fingers extending directly east. But the terrain elevation varies by at least 50 m at distances of 1 km in all directions. The height of the site location is estimated to be 430 m above sea level by the topography of the site (Sorbjan et al., 1991, Fig. 1). Sorbjan et al. (1991) analyzed the SODAR profiles of C_T^2 and $\sigma_{\rm w}^2$ in the convective boundary layer by using local similarity theory and deduced the surface SHF. They also presented the surface SHFs derived using the EC and turbulence variance methods for comparison (Table 3 and Table 4). The height z_i is defined as the height where the value of C_T^2 achieves a relative maximum and z_0 is defined as the level where the value of C_T^2 achieves a characteristic minimum (Appendix A). z_i and z_0 are inferred from C_T^2 profiles in Sorbjan et al. (1991) and are listed in Table 4 with other related parameters. The values of C_T^2 and σ_w^2 used in Eq. (10) were also read from the profiles in Sorbjan et al. (1991). Because the C_T^2 profile in Sorbjan et al. (1991) had not been corrected for atmospheric absorption attenuation, excess attenuation and wind effect, the values of C_T^2 are underestimated. To obtain accurate estimates, correction for these attenuation factors is necessary, especially for atmospheric absorption. To calculate the atmospheric absorption coefficient, the equations in the new ISO standard were used (ISO 9613-1, 1993). The atmospheric pressure is estimated to be 965 hPa according to the site level above the sea. The relative humidity (RH) is derived from the vapor pressure (Table 4). These are necessary for the calculation of the atmospheric absorption coefficient. The results of the calculation are 0.0022 and 0.0024 (Np m^{-1}) for time 1000 UTC and 1145 UTC respectively. The methods for the estimation of excess attenuation and wind effect are the same as those noted in section 3.1. The related SODAR parameters are the frequency ($f = 2000$ Hz), the antenna diameter ($d = 1.6$ m), and the beam width about 10 degrees. The C_V^2 profiles, which are necessary for the calculation of excess attenuation, were converted from the $\sigma_{\rm w}^2$ profiles according to the following relationship (Appendix B):

$$C_V^2 = 0.636 z^{-2/3} \sigma_{\rm w}^2 \,. \tag{13}$$

For the purpose of comparison with other results, we only deal with the data lower than about the zero-heat-flux layer.

Table 5. Deduced sensible heat flux profile and the corresponding profiles of C_T^2, corrected C_T^2 and σw^2 [based on data from Sorbjan et al. (1991)], 1145–1200 UTC 27 June 1987.

Height (m)	C_T^2 (K^2 m$^{-2/3}$)	C_T^2 corrected	σ_w^2 (m^2 s^{-2})	SHF (K m s^{-1})
80	0.00234	0.0043	0.195	0.056
110	0.00108	0.00234	0.207	0.042
140	0.00048	0.00122	0.234	0.031
170	0.00025	0.00075	0.313	0.026
200	0.00021	0.00075	0.340	0.023
230	0.00020	0.00097	0.291	0.020
260	0.00018	0.00088	0.235	0.014
290	0.00015	0.00097	0.159	0.008
320	0.00014	0.00114	0.177	0.005
350	0.00012	0.00122	0.196	0
380	0.00015	0.00195	0.202	−0.007

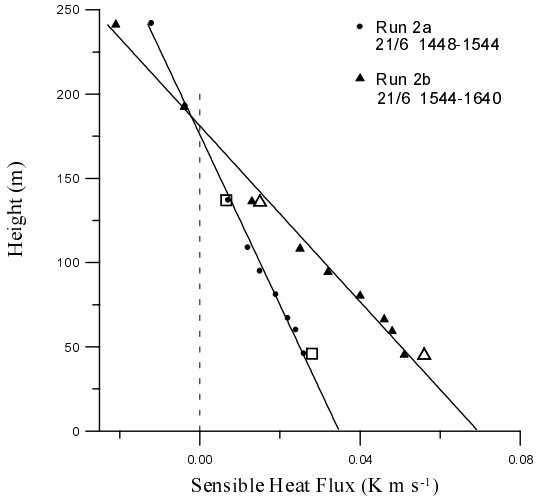

Fig. 3. Sensible heat flux profiles deduced from Eq. (11) under convective conditions [based on data from Moulsley et al. (1981)]: □—directly measured value of the SHF for dataset of Run 2a; △—for data of Run 2b.

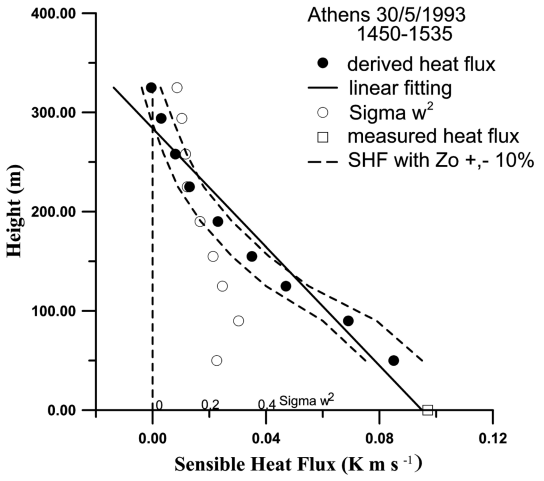

Fig. 4. Deduced sensible heat flux profile, Athens, 30 May 1993.

5. Results and discussion

5.1 *Results deduced from the data of Moulsley et al. (1981)*

The values of z_i and z_0 (Table 2) deduced from Eq. (11) for datasets of Runs 2a and 2b are obviously smaller than those of a typical mixed layer at the same time period. It was cloudy on 20 June 1977 and 21 June 1977 and the amount of low cloud were 8/8 and 7/8 respectively Moulsley et al. (1981). We can see from the facsimile record (Fig. 2) that the convective activity was not strong. Only a few thermal plumes reach up to about 180 m, most of them being under about 120 m. So, the small values of z_i and z_0 are reasonable. Comparing with the value of z_0 for Run 2a, the increase of z_0 for Run 2b is slight. This result matches the time variation of the thermal plume in

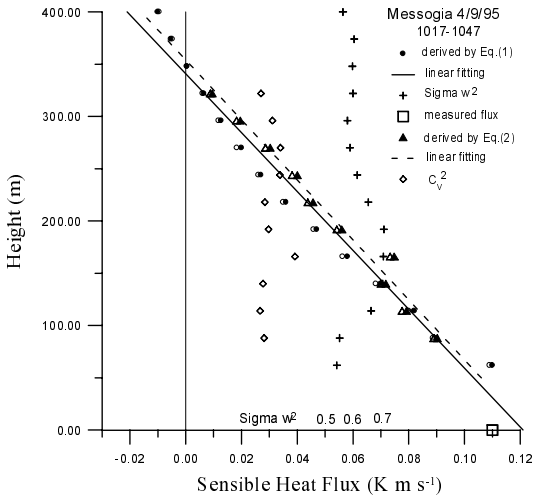

Fig. 5. Deduced sensible heat flux profiles, Messogia Plain, 4 September 1995.

Fig. 2, which shows that the convective activity of Run 2b (1544 to 1640; the right half of Fig. 2) was just stronger than that of Run 2a (1448 to 1544; the left half of Fig. 2). The SHFPs deduced from Eq. (11) show a linear decrease of SHF with height under convective conditions (Fig. 3). The digital data of SHFP and corresponding profiles of and are listed in Table 5. The surface SHF, H_0, can be derived from the intersection of the solid line with the x-axis. The values of H_0 for Runs 2a and 2b are 0.035 K m s^{-1} and 0.069 K m s^{-1} respectively.

5.2 *Results deduced from the data of Kalogiros et al. (1999)*

Figure 4 presents the deduced sensible heat flux profile from the data sets observed at Athens, 30 May 1993, and Fig. 5 presents the same results but observed at Messogia Plain, 4 September 1995. The possible errors of deduced SHF due to $\pm 10\%$ of z_0 are also plotted as the range of dashed lines. The linearity of SHFP on 30 May 1993 (Fig. 4) is not as good as that on 4 September 1995 (Fig. 5). The former experiment was carried out on complex terrain and dominated by a local sea breeze, whereas the latter took place at a flat location with no sea breeze. The facsimile record on 30 May 1993 (Fig. 6) shows a structure of the inner boundary layer, while that on 4 September 1995 shows a structure of the mixed layer (Fig. 7). The SHFP in Fig. 4 looks like a combination of two parts. Notice that the distance from the National Observatory of Athens (the site of the experiment on 30 May 1993) to the nearest southwest coastline is just about 6 km (Kalogiros et al., 1999, Fig. 1). The upper part of the SHFP may reflect the characteristic of turbulence over the offing, while the lower part reflects the characteristic of local turbulence. The surface SHF value derived from the SHFP on 30 May 1993 equals 0.095 K m s^{-1} (see Fig. 4), while the surface SHF value deduced from the linear fit of the five points between 50 m and 190 m in the SHFP equals 0.108 K m s^{-1}. The latter is just about 10% larger than the directly measured value (Table 3). Using the four points between 225 m and 325 m yields a very good fitted line, and derives a SHF value of 0.043 K m s^{-1}. In comparison with the surface SHF value of 0.108 K m s^{-1}, which is derived from a lower five points, the lower value of 0.043 K m s^{-1} could represent the surface SHF on the offing during the sea breeze event. Manghnani et al. (2000) observed SHF ranging from 5–35 W m^{-2}, corresponding to 0.004–0.028 K m s^{-1} in kinematics heat flux units over open ocean in the Indian Ocean Experiment (INDOEX), and found the boundary layer height was approximately linearly related to the sensible heat flux at the ocean surface.

Figure 5 shows two SHFPs for the same time interval, which are deduced from Eqs. (10) and (11) respectively. Their linear fitted lines are much closer to each other. The values of the surface SHF by linear extrapolation of these two SHFPs are 0.121 and 0.123 K m s^{-1} respectively. The difference of these two estimates may be smaller than the measurement errors. For comparison with the results from Fairall's model (1987), the corresponding values of SHF are illustrated in Fig. 5 with open circles and triangles. The values of derived from Fairall's model (1987) are slightly smaller than those from Eq. (12), the differences being around 2%–8% in this case study. The corresponding values of the surface SHF by linear extrapolation are 0.119 and 0.121 K m s^{-1} respectively.

The surface SHFs derived from SHFPs in Figs. 4 and 5 agree well with those measured using EC (Table 3). The result of deduction of SHFPs shows the direct estimate of z_i, using the echo intensity profile, is reasonable. To ignore the upper part of the σ_w^2 profile for the case on 30 May 1993, while Kalogiros et al. (1999) used the fitted σ_w^2 profile to estimate z_i, caused an underestimated value of z_i. The shortcoming of the retrieval of SHFP here is the assumption of the shape of the C_T^2 profiles, Eq. (12), but the results show that the assumption for this case does not bring about a large error.

5.3 *Results deduced from the data of Sorbjan et al. (1991)*

Four deduced SHFPs, among which two are based on the original data and the other two by using the corrected C_T^2 profiles, are plotted in Fig. 8. The related digital data are listed in Table 6. The values of surface SHF derived from the linear fit of original SHFPs equal 0.037 and 0.044 K m s^{-1} for the time 1000 and 1145 respectively. Those derived from the linear fit of corrected SHFPs equal 0.055 and 0.064 K m s^{-1} for the time 1000 and 1145 respectively. The latter is in agreement with the value of 0.067, which was deduced by Sorbjan et al. (1991) from SODAR data, but is still much smaller than that measured using the EC method (Table 3). We found each of the SHFPs at the time 1145 UTC can be separated into two linear parts, one from 80–140 m and the other from 170–380 m. The change of the profile's slope from 140 m high can be explained by the experimental site being located on hilly terrain. The surrounding non-uniform terrain and the small flat area of the site may cause a local turbulent characteristic in the lower part of the mixed layer and advection turbulence in the upper part. The height of the interface of these two parts depends on the size of the flat area, the wind and vegetation etc. Concerning the different characteristics of turbulence

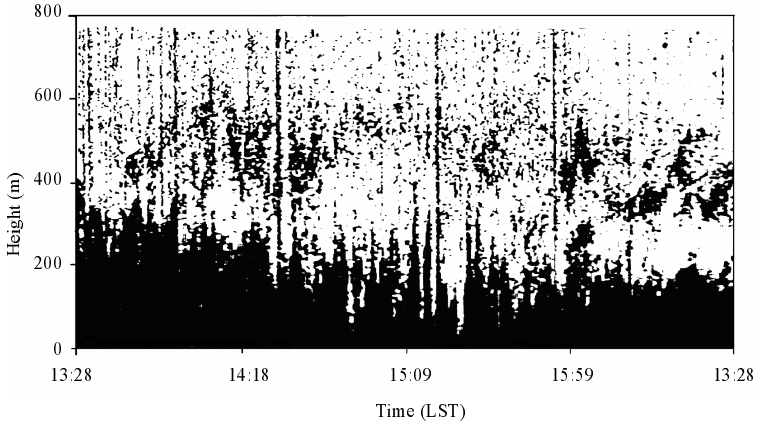

Fig. 6. Echo pattern, Athens, 30 May 1993, from Kalogiros et al. (1999).

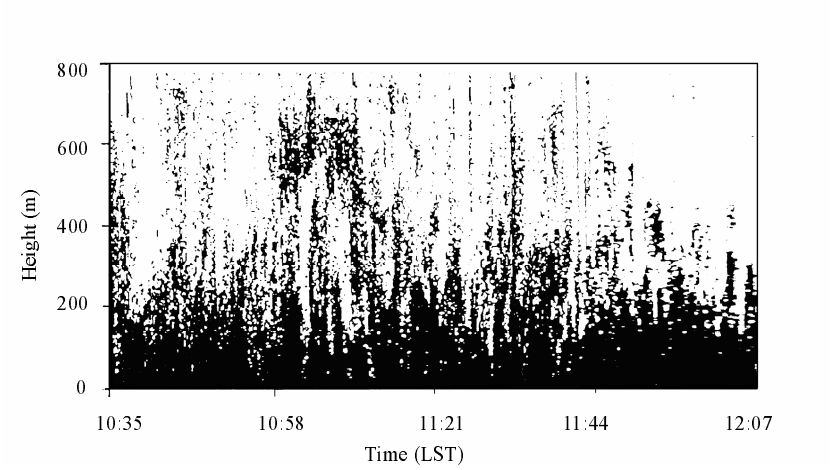

Fig. 7. Echo pattern, Messogia Plain, 4 September 1995, from Kalogiros et al. (1999).

in the lower part and upper part of the mixed layer, we took a linear fit of the lowest three points of the corrected SHFP at time 1145 UTC in Fig. 8 and derived the surface SHF value of 0.089 K m s^{-1}. It is larger than the value of 0.067 K m s^{-1} deduced from the local similarity theory and close to the value of 0.099 K m s^{-1} measured using the EC method (Table 3). If the C_T^2 and σ_w^2 profiles reach down into the surface layer, we believe the surface SHF derived from the corrected SHFP will agree with that measured using the EC method.

6. Representative of surface SHF and related similarity relationship

The deduced SHFPs for the flat area in this paper show a good linear decrease with height under convective conditions (Figs. 3 and 5). They make sense either on clear days (Figs. 5 and 7) or on cloudy days (Figs. 2 and 3). It is easy to obtain the surface SHF from SHFPs by linear extrapolation down to the x-axis. The surface SHFs derived from the SHFPs for Kalogiros et al. (1999) agree well with the direct measured values (Table 3). Even on cloudy days, the differences between the surface SHFs deduced from SHFPs (Fig. 3) and those of linear extrapolation of two direct measured points at 46 m and 137 m height (Table 2) are just about 10%. A surface SHF derived from a SODAR SHFP with a good linearity has a good representative spatially and temporally. The values of surface SHF deduced from SHFPs, the direct estimates (EC) and other indirect estimates [C_V^2 profile method, σ_w^2 profile method, Kalogiros et al. (1999)] are listed in Table 3 for comparison. The difference between the derived and direct measured surface SHF in complicated terrain (Figs. 4 and 8) and under complicated meteorology conditions (Figs. 4 and 6) are large. Also, the slopes of corresponding deduced SHFPS changed from a certain level. In this case the representative of surface SHF is no good for both the derived and direct measured values, even though the latter may be accurate.

Table 6. Deduced sensible heat flux profiles and the profiles of C_T^2, corrected C_T^2 and C_V^2 [based on data from Moulsley et al. (1981)], 1448–1640 UTC 21 June 1977.

Run	Height (m)	C_T^2 ($K^2\ m^{-2/3}$)	C_T^2 corrected	C_V^2 ($m^{4/3}\ s^{-2}$)	SHF ($K\ m\ s^{-1}$)
2a	46	0.00063	0.00082	0.034	0.026
	60	0.0006	0.00080	0.027	0.024
	67	0.0005	0.00067	0.025	0.022
	81	0.0004	0.00055	0.024	0.019
	95	0.0003	0.00043	0.022	0.015
	109	0.00022	0.00033	0.023	0.012
	137	0.00015	0.00025	0.024	0.007
	193	0.00008	0.00017	0.021	−0.0036
	242	0.00005	0.00014	0.015	−0.012
2b	46	0.00081	0.0011	0.039	0.051
	60	0.0007	0.00097	0.035	0.048
	67	0.00063	0.00088	0.033	0.046
	81	0.00049	0.00071	0.032	0.040
	95	0.00035	0.00053	0.031	0.032
	109	0.00025	0.00039	0.029	0.025
	137	0.00016	0.00027	0.023	0.013
	193	0.00011	0.00025	0.019	−0.0039
	242	0.00008	0.00025	0.016	−0.021

A similarity relationship of SHF for the mixed layer is:

$$\overline{w'T'} = H_0 \left(1 - \beta \frac{z}{z_i}\right) , \tag{14}$$

where

$$\beta = 1 - \frac{H_{\rm top}}{H_0} ,$$

$H_{\rm top}$ is the SHF at the top of the mixed layer (Stull, 1988). Measuring $H_{\rm top}$, however, is difficult. Notice a surface layer similarity relationship:

$$\sigma_{\rm w} = 1.9 U_* \left(-\frac{z}{L}\right)^{1/3} , \tag{15}$$

where u_* is the friction velocity and L is the Obukhov length; $L = -u_*^3\theta/gkH_0$, where k is the von Karman constant. Assuming Eq. (15) is valid in the middle and lower part of the mixed layer and inserting it and Eq. (12) into Eq. (10) yields:

$$\overline{w'T'} = \chi H_0 \frac{z_0 - z}{z_1} , \tag{16}$$

where χ is a coefficient. Comparing Eq. (16) with Eq. (14), χ must equal z_i/z_0, and β in Eq. (14) then equals z_i/z_0. The coefficient β in Eq. (14) then has a physical meaning of the ratio of the mixed layer height to the zero-heat-flux layer height. A more clear expression can be rewritten as follows:

$$\overline{w'T'} = -\frac{H_0}{z_0} z + H_0 . \tag{17}$$

Using the derived and/or direct measured surface SHF in Figs. 3 and 5 to get linear SHFPs by Eq. (17), we found they agree well with the linear fit of deduced SHFPs. The case studies show that Eq. (17) is valid for the mixed layer (not the inner boundary layer) from the surface up to the zero-heat-flux layer in a flat area, but not for complicated terrain and/or meteorological conditions. From another point of view, as the mixed layer height z_i does not appear in the equation and the entrainment processes produces a downward entrainment flux of heat at the top of the mixed layer, Eqs. (17) and (14) are believed not to be valid in the upper part of the mixed layer.

7. Conclusions

Six sets of SODAR data and surface layer data have been examined for the verification of SHF expressions, Eqs. (10) and (11). The problem of shortage at some parameters in these data was solved to meet the needs of these expressions. The good linear decease of SHF with height happened only on a large flat area under steady convective conditions. The SHFPs are sometimes composed of two linear parts, which were found to be related to the inhomogeneities in upwind topography or the local circulation (sea breeze). In these cases, the lower part reflects the local turbulence and the upper part reflects the advective turbulence. The values of the surface SHF derived from the linear extrapolation of the SHFPs agreed well with those measured using EC only in the well-mixed layer and on a

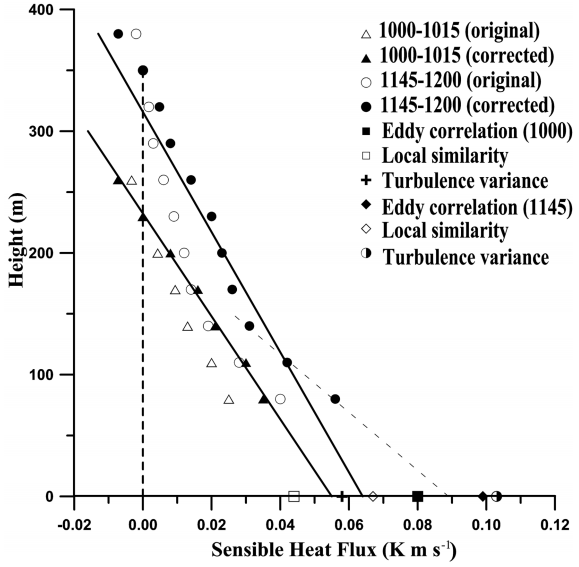

Fig. 8. Sensible heat flux profiles deduced from SODAR data of Sorbjan et al. (1991) and derived surface sensible heat fluxes. Other surface sensible heat fluxes measured or estimated with different methods are plotted for comparison.

flat area. However, for complicated terrain (Sorbjan et al., 1991), with the tendency of the SHFP to the surface, a surface SHF closer to the direct measured value can be derived. The representative of surface SHF in the complicated topography is then a problem for attention. The linearity of SHFP deduced from SODAR data may be utilized as an indicator of the representative of the surface SHF.

As predicted by the author (Pan, 2002) that the proposed method provides estimates of SHF "under less restrictive boundary conditions", the cases analyzed in this paper shows the SHF expressions in Eqs. (10) and (11) are valid from the surface layer up to around the zero-heat-flux layer for different terrain and meteorological conditions in a dry convective boundary layer. It may not, however, hold when wind shear exists.

The similarity relationship Eq. (17) can be used for the well-mixed layer up to the middle part with an acceptable accuracy and has the advantage of only two governing parameters, of which one can be measured by EC and the other can be inferred by the echo pattern of commercial SODAR. It does not, however, hold for complicated terrain. Theoretically, the valid area using Eqs. (10) and (11) in the boundary layer will be larger than the area validated in this paper and not restricted only to the mixed layer. But what about the distribution of local homogeneous and isotropic turbulent fields in the boundary layer? Does the upper part of the boundary, in which the entrainment effect plays its role, meet our needs? Not enough is yet known to answer these questions.

By this study, SODAR is proposed to be an independent piece of remote sensing equipment that provides SHFPs which have a better spatial and temporal representative than those collected by in situ direct measurements and by the scintillation method, which cannot obtain SHFPs. The sequential SHFPs and corresponding facsimile records will be helpful in boundary layer diagnoses and the validation of atmospheric models.

The validation of Eqs. (10) and (11) here is limited by using a few short periods of data which are taken from different experiments designed for different aims. Further verification requires the careful designing of an experiment which should cover:

(1) direct measurement of surface meteorological parameters, including temperature, humidity, pressure, wind etc., and the recording of weather conditions;

(2) direct measurement of the temperature and velocity spectrum and related calculation of turbulent parameters, including $C_T^2, -\sigma_{\rm w}^2, H_0$, and u_* with tower and tethered balloon instruments, plus $H_{\rm top}$ if possible;

(3) a calibrated Dopller SODAR system; and

(4) a proper experiment field with a flat area and hopefully a neighboring different terrain.

Under these experimental conditions, the physical process of vertical transportation of scalar parameters can be studied in advance, and the new remote sensing method with SODAR and the top-down and bottom-up model (Fairall, 1987) may provide further possible verification and improvements.

Acknowledgements. We are grateful for lots of valuable comments on the earlier draft of this manuscript provided by two anonymous reviewers and the editors of this journal. The study is partially supported by the National Natural Science Foundation of China (NSFC) (Grant Nos: 40575001, 40775002) and the National High Technology Research and Development Program of China (863 Major Project, Grant No: 2006AA06A306).

APPENDIX A

The Value of C_T^2 at Zero-Heat-Flux Layer

According to the turbulence closure K-theory and mixing length theory:

$$\overline{w'\theta'} = -K_h \frac{\partial \bar{\theta}}{\partial z} \,. \tag{A1}$$

In the lower convective mixed layer, SHF ($\overline{w'\theta'}$) decreases with increasing height (Stull, 1988), and fi-

nally reaches zero at a specific height z_0 in the mixed layer. In this layer the potential temperature reaches its minimum for presence of the heating of the surface layer and the warming of the entrainment layer and free atmosphere. Thus, within this layer, we must have:

$$\left.\frac{\partial\bar{\theta}}{\partial z}\right|_{z=z_0} = 0 \,. \tag{A2}$$

For a monostatic SODAR, the acoustic back scattering cross section $\sigma(\pi)$ is proportional to the structure parameter of temperature fluctuation C_T^2 in a statically stable and dry atmosphere (Singal, 1989):

$$\sigma(\pi) = 0.00408k^{1/3}\frac{C_T^2}{T_0^2} \,. \tag{A3}$$

Another expression of acoustic back scattering cross section is given by Singal (1989) in terms of the gradient Richardson number Ri and potential temperature gradient as follows:

$$\sigma(\pi) = 0.165\frac{k^{1/3}}{T_0^2}k_h^{2/3}\left(\frac{Ri}{K_m/K_h - Ri}\right)^{1/3}\left(\frac{d\theta}{dz}\right)^{5/3} \,. \tag{A4}$$

Hence, from Eqs. (A3) and (A4) we know C_T^2 should be proportional to $(d\theta/dz)^{5/3}$, with the conditions of Eq. (A2) we have the conclusion:

$$C_T^2\big|_{z=z_0} = 0 \,. \tag{A5}$$

In real measurements, for presence of side beams of SODAR, a minimum of C_T^2 can be observed:

$$C_T^2\big|_{z=z_0} = C_{T\min}^2 \,. \tag{A6}$$

APPENDIX B

The Relationship Between C_V^2 and σ_w^2 Under the Condition of Kolmogorov's Local Homogeneous Isotropic random field

According to Tatarskii (1961), under the conditions of Kolmogorov's local homogeneous isotropic random field, the one dimension spectrum of energy can be deduced from structure functions as follows:

$$E(\kappa) = \frac{\Gamma(5/3)\sin(\pi/3)}{2\pi}C_V^2\kappa^{-5/3} \,, \tag{B1}$$

where κ is the wave number. The one dimension spectrum can also be expressed by the von Karman spectrum as:

$$E(\kappa) = \frac{\Gamma(5/6)L_0}{3\sqrt{\pi}\Gamma(1/3)(1+\kappa^2L_0^2)^{5/6}}\sigma_w^2 \,, \tag{B2}$$

where L_0 is the outer scale of turbulence. Combine these two equations and let $\kappa = 1$, yields:

$$C_V^2 = \frac{0.636L_0}{(1+L_0^2)^{5/6}}\sigma_V^2 \,. \tag{B3}$$

For the variance of vertical velocity, $L_0 \approx z$ and $L_0 \gg 1$, we have:

$$C_V^2 = 0.636z^{-2/3}\sigma_w^2 \,. \tag{B4}$$

REFERENCES

Asimakopoulos, D. N., C. G. Helmis, and J. Michopoulos, 2004: Evaluation of SODAR methods for the determination of the atmospheric boundary layer mixing height. *Meteor. Atmos. Phys.*, **85**, 85–92.

Bian, L., X. Xu, L. Lu, Z. Gao, M. Zhou, and H. Liu, 2003: Analyses of turbulence parameters in the near-surface layer at Qamdo of the Southeastern Tibetan Plateau. *Adv. Atmos. Sci.*, **20**(3), 369–378.

Chintawongvanich, P., R. Olsen, and C. A. Biltoft, 1989: Intercomparison of wind measurements from two acoustic Doppler Sodars, a laser Doppler Lidar, and in situ sensors. *J. Atmos. Oceanic Technol.*, **6**, 785–798.

Coulter, R. L., 1990: Minisodars—Applications and Potential. *Proc. 5th International Symposium on Acoustic Remote Sensing of the Atmosphere and Oceans*, New Delhi, India, 88–96.

Coulter, R. L., and M. L. Wesley, 1980: Estimates of surface heat flux from Sodar and laser scintillation measurements in the unstable boundary layer. *J. Appl. Meteor.*, **19**, 1209–1222.

Fairall, C. W., 1987: A top-down and bottom-up diffusion model of C_T^2 and C_Q^2 in the entraining convective boundary layer. *J. Atmos. Sci.*, **44**, 1009–1017.

Finkelstein, P. L., J. C. Kaimal, J. E. Gaynor, M. A. Graves, and T. J. Lockhart, 1986: Comparison of wind monitoring system. Part II: Doppler Sodars. *J. Atmos. Oceanic Technol.*, **3**, 583–593.

Gaynor, J. E., 1977: Acoustic Doppler measurements of atmospheric boundary layer velocity structure functions and energy dissipation rates. *J. Appl. Meteor.*, **16**, 148–155.

Georges, T. M., and S. F. Clifford, 1974: Estimating refractive effects in acoustic sounding. *The Journal of the Acoustical Society of America*, **55**, 934–936.

Hill, R. J., G. R. Ochs, and J. J. Wilson, 1992: Measuring surface-layer fluxes of heat and momentum using optical scintillation. *Bound.-Layer Meteor.*, **58**, 391–408.

ISO 9613-1, 1993: Acoustics-attenuation of sound during propagation outdoors—Part 1: Calculation of the attenuation of sound by atmospheric absorption. International Organization for Standardization, Geneva, Switzerland.

Kalogiros, J. A., C. G. Helmis, D. N. Asimakopoulos, and P. G. Papageorgas, 1999: Estimation of ABL parameters using the vertical velocity measurements

of an acoustic sounder. *Bound.-Layer Meteor.*, **91**, 413–449.

Keder, J., T. Foken, W. Gerstmann, and V. Schindler, 1989: Measurement of wind parameters and heat flux with the Sensitron Doppler Sodar. *Bound.-Layer Meteor.*, **46**, 195–204.

Kristensen, L., and J. E. Gaynor, 1986: Errors in second moments estimated from monostatic Doppler Sodar winds. Part 1: Theoretical description. *J. Atmos. Oceanic Technol.*, **3**, 523–528.

Li, M., Y. Ma, W. Ma, Z. Hu, H. Ishikawa, Z. Su, and F. Sun, 2006: Analysis of turbulence characteristics over the northern Tibetan Plateau area. *Adv. Atmos. Sci.*, **23**(4), 579–585.

Manghnani, V., S. Raman, D. S. Niyogi, V. Parameswara, J. M. Morrison, S. V. Ramana, and J. V. S. S. Raju, 2000: Marine boundary-layer variability over the Indian Ocean during INDOEX (1998). *Bound.-Layer Meteor.*, **97**(3), 411–430.

Meijninger, W. M. L., O. K. Hartogensis, W. Kohsiek, J. C. B. Hoedjes, R. M. Zuurbier, and H. A. R. De Bruin, 2002: Determination of area-averaged sensible heat fluxes with a large aperture scintillometer over a heterogeneous surface-flevoland field experiment. *Bound.-Layer Meteor.*, **105**, 37–62.

Moulsley, T. J., D. N. Asimakopoulos, R. S. Cole, B. A. Crease, and S. J. Caughey, 1981: Measurement of boundary layer structure parameter profiles by acoustic sounding and comparison with direct measurement. *Quart. J. Roy. Meteor. Soc.*, **107**, 203–230.

Neff, W. D., 1975: Quantitative evaluation of acoustic echoes from the planetary boundary layer. NOAA Technical Report, ERL 322-WPL 38, 34pp.

Ostashev, V. E., 1994: Sound propagation and scattering in media with random inhomogeneities of sound speed, density and medium velocity. *Waves in Random Media*, **4**(4), 403–428.

Pan, N. X., 1997: Determination of the turbulent structure parameters. *Acoustic Remote Sensing Applications*, S. P. Singal, Ed., Narosa Publishing House, New Delhi, India, 179–190.

Pan, N. X., 2002: Expressions of sensible heat flux based on a dimensional analysis. *J. Atmos. Oceanic Technol.*, **19**, 1163–1169.

Pan, N. X., 2003: Excess attenuation of an acoustic beam by turbulence. *The Journal of the Acoustical Society of America*, **114**(6), 3102–3111.

Pan, N. X., and Y. Zheng, 1986: Wind effect on measurement of wind velocity with Doppler Sodar. *Acta Scientiarum Naturalium Universitatis Pekinensis*, **1**, 98–105. (in Chinese)

Panofsky, H. A., H. Tenekes, and D. H. Lenschow, 1977: The characteristics of turbulence volocity components in the surface layer under convective conditions. *Bound.-Layer Meteor.*, **11**, 355–361.

Singal, S. P., 1989: Acoustic sounding stability studies. *Air Pollution Control.* Vol. 2, *Encyclopedia of Environment Control Technology*, P. N. Cheremisinoff, Ed., Gulf Publishing, Houston, USA, 1003–1061.

Sisterson, D. L., and R. L. Coulter, 1979: Sodar Calibration Method. Argonne National Laboratory Radiological and Environmental Division Annual Report, ANL-78-65, Pt. IV, 7–18.

Sorbjan, Z., R. L. Coulter, and M. L. Wesely, 1991: Similarity scaling applied to sodar observations of the convective boundary layer above an irregular hill. *Bound.-Layer Meteor.*, **56**, 33–50.

Spizzichino, A., 1974: The refraction of acoustic waves in the atmosphere and its effect on Sodar wind measurements. *Annals of Telecommunications*, **29**, 301–310.

Stull, R. B., 1988: *An Introduction to Boundary Layer Meteorology.* Kluwer Academic Publishers, 666pp.

Tatarskii, V. I., 1961: *Wave Propagation in a Turbulent Medium.* R. A. Silverman, Trans., McGraw-Hill Book Company, Inc., New York, 285pp.

Thiermann, V., and H. Grassl, 1992: The measurement of turbulent surface layer fluxes by use of bichromatic scintillation. *Bound.-Layer Meteor.*, **58**, 367–389.

Tsvang, L. R., 1969: Microstructure of temperature fields in the free atmosphere. *Radio Science*, **4**, 1175–1177.

Vogt, S., and P. Thomas, 1994: Estimation of the sensible heat flux and the temperature structure parameter by sodar and sonic anemometer: An intercomparison. *Journal of Remote Sensing*, **15**(2), 507–516.

Weill, A., L. Eymard, M. E. Lequere, C. Klapisz, F. Baudin, and P. Van Grunderbeeck, 1978: Investigations of the planetary boundary layer with an acoustic Doppler sounder. *Proc. 4th Symposium on Meteorological Observations and Instrumentation*, American Meteorological Society, Denver, Colo., 10–14 April, 415–421.

Weill, A., C. Klapisz, B. Strauss, F. Baudin, C. Jaupart, P. V. Grunderbeeck, and J. P. Goutorbe, 1980: Measuring heat flux and structure functions of temperature fluctuations with an acoustic doppler sodar. *J. Appl. Meteorol.*, **19**, 199–205.

Wyngaard, J. C., 1990: Scalar fluxes in the planetary boundary layer-theory, modeling, and measurement. *Bound.-Layer Meteor.*, **50**, 49–75.

Wyngaard, J. C., and M. A. LeMone, 1980: Behavior of the refractive index structure parameter in the entraining boundary layer. *J. Atmos. Sci.*, **37**, 1573–1585.

Zhou, M., N. Lu, Y. Chen, and S. Li, 1981: The lump structure of turbulent field in atmospheric boundary layer. *Scientia Sinica*, **24**(12), 1705–1716.